IMAGE FIELDS IN THE RECTANGULAR VACUUM VESSELS OF THE ISIS SYNCHROTRON

B.G. Pine, ISIS, RAL, STFC, UK and JAI, Oxford, UK
C.M. Warsop, ISIS, RAL, STFC, UK

Abstract

ISIS is the pulsed spallation neutron source based at Rutherford Appleton Laboratory in the UK. Operation is based on a 50 Hz, 800 MeV proton synchrotron, accelerating up to 3×10^{13} protons per pulse, which provides beam to two target stations. Space charge effects contribute significantly to beam loss. Fields from the intense beam interact strongly with their environment. At ISIS the vacuum vessel is rectangular and profiled to follow the shape of the design beam envelope.

Past studies have suggested that closed orbit induced image fields may contribute to beam loss under certain conditions. Image fields for parallel plate and rectangular geometries are reviewed, in particular their expansion as power series is determined. A simulation tool has been developed for particle tracking with space charge. The code contains both Fast Fourier Transform and Finite Element Analysis based field solvers, which have been used here to test the range of validity for the power series expansions for centred and off-centred beams.

These expansions are then used to determine driving terms for the transverse beam motion. Of particular interest for ISIS is the resonant behaviour of beams with a harmonic closed orbit, which can be compared with the output of beam tracking simulations.

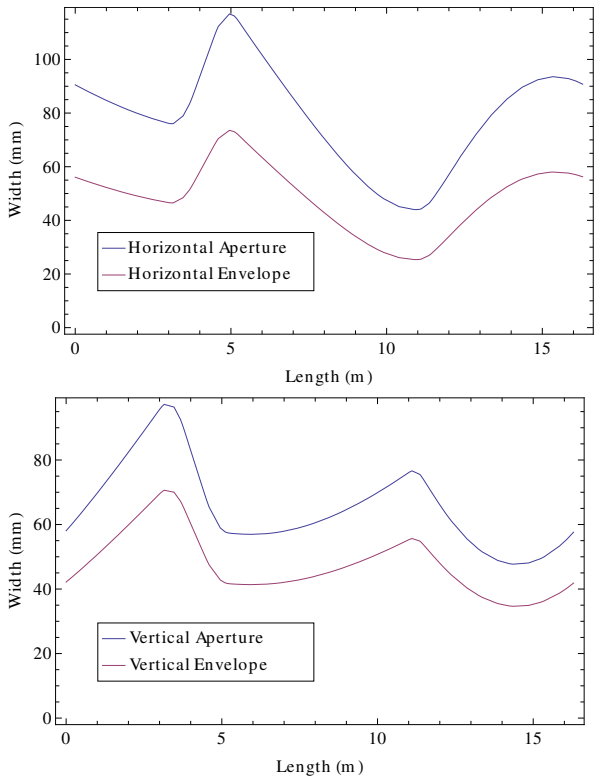

Figure 1: Apertures and envelopes for one super period of the ISIS RCS: (top) horizontal, (bottom) vertical.

INTRODUCTION

At the highest intensities it is believed that image forces from off-centred beams can contribute to losses on ISIS [1,2]. These beam losses are difficult to isolate during normal operation of the facility. Therefore a program of analysis and simulation has been established in order to describe the effect of image forces and try to estimate the level of beam loss they could potentially cause. In the future it is hoped that a better understanding of the image forces may allow them to be identified experimentally. Analyses for parallel plate and rectangular geometry including centred and off-centred beams are reviewed. The results are then compared with the output of particle-in-cell (PIC) simulations.

The ISIS rapid cycling synchrotron (RCS) accelerates a high intensity beam at a fast repetition rate of 50 Hz. The synchrotron has a circumference of 163 m. It is composed of 10 super periods, with specialised sections for injection, extraction and collimation. The peak incoherent tune shifts are 0.5 or larger in both planes. Many different loss mechanisms may contribute to beam loss at any particular point in the machine cycle, especially during the time between injection and bunching of the beam, when space charge forces peak. In order to gain insight into the individual loss processes it is helpful to separate out different effects to study. For the purpose of the present paper attention is focused purely on the transverse plane, and in particular a geometrical approach to the image forces.

ISIS has rectangular vacuum vessels and RF shields whose cross section runs parallel to the design beam envelope in both planes (Figure 1). Of particular interest for ISIS are the higher order image terms due to off-centered beams. It has been suggested that these may affect beam loss at the highest intensities [1].

IMAGE FIELDS IN PARALLEL PLATE AND RECTANGULAR GEOMETRY

Image Terms due to Laslett

Following Laslett [3], parallel plate geometry is used as an approximation to rectangular. For a beam centred at y_1 between two infinite parallel plates at $\pm h$ and a field point at y as shown in Figure 2, there are an infinite series of images above and below the beam. Conformal mapping may be used to transform to a new system where the images are

ISBN 978-3-95450-173-1

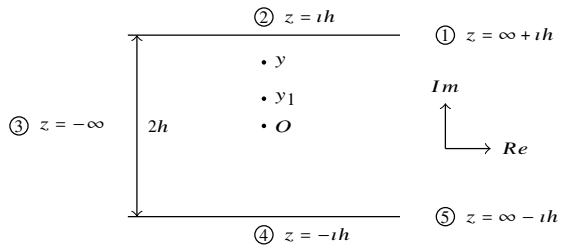

Figure 2: Parallel plate geometry before conformal mapping.

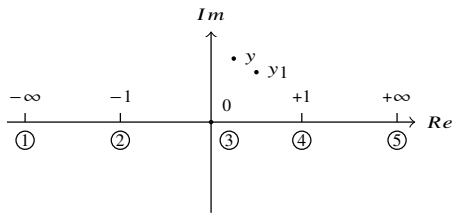

Figure 3: Parallel plate geometry after a conformal mapping into the real axis.

easier to obtain. The transformation $z' = e^{\pi(z+\imath h)/2h}$ carries points 1 - 5 from Figure 2 into the real number line in z' as shown in Figure 3.

The potential due to a line charge is $W = -2\lambda \ln|z|$

$$W = -2\lambda(\ln\left|e^{\imath\pi(y+h)/2h} - e^{\imath\pi(y_1+h)/2h}\right| - \ln\left|e^{\imath\pi(y+h)/2h} - e^{-\imath\pi(y_1+h)/2h}\right|).$$

The real potential is obtained from this

$$U = -2\lambda \ln\left|\frac{\sin(\pi y/2h) - \sin(\pi y_1/2h)}{1 + \cos(\pi(y+y_1)/2h))}\right|. \quad (1)$$

Equation 1 is exact. The answer is then approximated using power series expansions. Expanding to second order

$$U \simeq -2\lambda\left(\ln\left|\frac{\pi(y-y_1)}{4h}\right| + \frac{\pi^2(y^2+4yy_1+y_1^2)}{48h^2}\right).$$

The first term is the potential of a bare line charge, the second is Laslett's expansion for images between parallel plates. While real, high intensity beams are not point like, the image terms are still a reasonable approximation if the beam is far enough away from the chamber wall.

If Laslett's image term is differentiated with respect to y we obtain the image component of the electric field

$$E_y \simeq -2\lambda\frac{\pi^2}{48h^2}(2y+4y_1).$$

Changing variables to $\bar{y} = y_1$ and $\hat{y} = y - y_1$ then gives

$$E_y \simeq -2\lambda\frac{\pi^2}{48h^2}(2\hat{y}+6\bar{y}).$$

Laslett's image co-efficients are divided by 4 to obtain $\epsilon_1 = \frac{\pi^2}{48}$ for images due to the offset of the field point from the centre of the beam (known as the incoherent term), and $\xi_1 = \frac{\pi^2}{16}$ for images due to the offset of the beam from the centre of the beam pipe (known as the coherent term), finally giving for the electric field due to images

$$E_y \simeq -4\frac{\lambda}{h^2}(\epsilon_1\hat{y} + \xi_1\bar{y}). \quad (2)$$

Expansion due to Baartman

Baartman [2] starts with Equation 1, but expands the power series to the 5th power to obtain

$$U \simeq -2\lambda(\ln\left|\frac{\pi(y-y_1)}{4h}\right| + \frac{\pi^2(y^2+4yy_1+y_1^2)}{48h^2} + \frac{\pi^4(7y^4+32y^3y_1+42y^2y_1^2+32yy_1^3+7y_1^4)}{23040h^4}).$$

Leaving out the term due to the free line charge and differentiating with respect to y to get E_y

$$E_y = \frac{\lambda\pi^2}{24h^2}(2y+4y_1) + \frac{\lambda\pi^4}{11520h^4}(28y^3+96y^2y_1+84yy_1^2+32y_1^3).$$

Baartman then rearranged this in terms of $\bar{y} = y_1$ and $\hat{y} = y - y_1$ to give

$$E_y = \frac{\lambda\pi^2}{24h^2}(2\hat{y}+6\bar{y}) + \frac{\lambda\pi^4}{11520h^4}(28\hat{y}^3+180\hat{y}^2\bar{y}+360\hat{y}\bar{y}^2+240\bar{y}^3)$$

$$= \frac{\lambda\pi^2\hat{y}}{12h^2} + \frac{\lambda\pi^2\bar{y}}{4h^2} + \frac{28\lambda\pi^4\hat{y}^3}{11520h^4} + \frac{\lambda\pi^4\hat{y}^2\bar{y}}{64h^4} + \frac{\lambda\pi^4\hat{y}\bar{y}^2}{32h^4} + \frac{\lambda\pi^4\bar{y}^3}{48h^4}.$$

The first two terms are Laslett's linear image terms. The others represent non-linear terms which are functions of both the distance of the field point from the beam centre, and the beam centre offset from the origin. It is these higher order terms that Rees, Prior [1] and Baartman suggested as a source of closed orbit image driven losses at ISIS.

Elliptical Function Solution due to Ng

Ng also uses conformal mapping to derive the potential but then uses elliptical functions, $K(k)$, to solve for the exact solution with a rectangular boundary [4, 5]. For a centred beam the elliptical functions simplify to (see Equation 3.109 from [5]):

$$sn\left(\frac{K(k')}{2}, k'\right) = \frac{1}{\sqrt{1+k}},$$
$$cn\left(\frac{K(k')}{2}, k'\right) = \frac{\sqrt{k}}{\sqrt{1+k}},$$
$$dn\left(\frac{K(k')}{2}, k'\right) = \sqrt{k}.$$

ISBN 978-3-95450-173-1

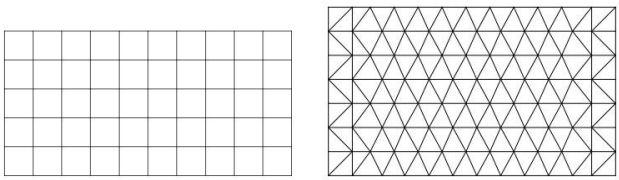

Figure 4: Mesh for Poisson solvers: (left) FFT solver using finite difference approach, (right) FEA solver using iterative relaxation.

The nome for rectangular geometry is $q = \mathrm{e}^{-2\pi\omega/h}$. The argument of the doubly periodic functions can be approximated if the ratio of the vacuum vessels satisfies certain conditions:

$$k^2 = 16q(1-8q+44q^2-192q^3+718q^4-2400q^5+7352q^6 - 20992q^7 + 56549q^8).$$

$$K(k) = \frac{\pi}{2}\left[1 + \frac{1}{4}k^2 + \frac{9}{64}k^4 + O(k^6)\right].$$

Following these steps a simple estimate may be made for the image co-efficient for a centred beam cf. Equation 2

$$\epsilon_1 = \frac{K^2(k)}{12}(1 - 6k + k^2).$$

SIMULATION MODEL

In this section the Poisson solvers are presented and some initial results demonstrated, then in the next sections they are used to investigate the different models that have been introduced. The simulation model allows the generation of a beam distribution in a rectangular boundary, and calculation of the resulting potential and electric fields. Two Poisson solvers were compared for this task, one using a rectangular mesh with a Fast Fourier Transform (FFT) solver and the other using a triangular mesh and a Finite Element Analysis (FEA) solver, see Figure 4. The solvers are from the beam tracking code, Set [6].

The FFT solver was originally created to solve for the potential of beam fields in the ISIS conformal vacuum vessel. The FEA solver was added to allow the calculation of beam fields in other geometries. Their main requirements are speed and accuracy, as normally they have to solve for beam potentials hundreds of times per simulated turn in the beam tracking code, Set. The FFT solver uses matrix methods to directly solve for the potential, while the FEA solver uses an iterative relaxation approach. For these simulations a KV beam distribution was used as it has a linear space charge force which can easily be compared with theory. 5×10^5 macro particles were used for each of the simulations as this number gave acceptably low statistical noise. Figure 5 (left) shows a scatter plot of the particles in a square aperture, while Figure 5 (right) shows a density plot of the same. Figures 6 and 7 show the potential and electric fields calculated from a KV beam in a square aperture. Figure 8 shows the horizontal and vertical fields on lines through

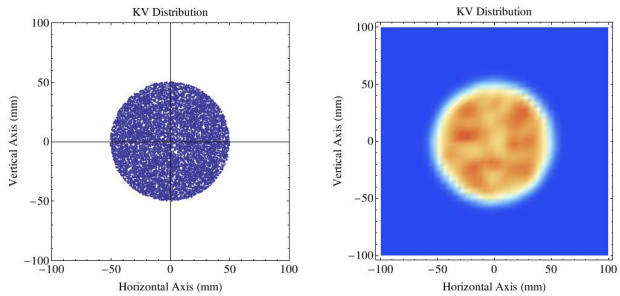

Figure 5: (Left) KV distribution in a square aperture showing 10^4 particles, (right) density plot of the KV distribution.

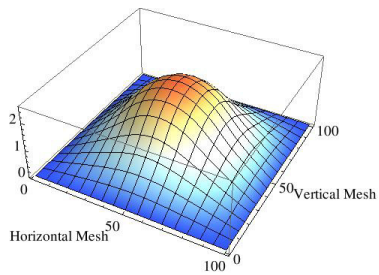

Figure 6: 3D plot of potential due to KV beam in square aperture, units ϵ_0 V.

the centre of the beam, compared with the calculated fields for a KV beam. There was an excellent level of agreement between the FFT and FEA solvers for both the obtained potential and fields, presented more fully elsewhere [7].

Results for Centred Beam

The range of validity for the parallel plate approximation was compared with the full rectangular geometry solution. In this case a centred beam was investigated, so only the image terms due to a centred beam were considered. An image co-efficient equivalent to Laslett's (Equation 2) could be obtained by taking the gradient of the electric field across the beam. A linear fit provided the best match to the image co-efficient. Baartman's expansion only adds very small terms to the solution for a centred beam. A set of simulations was run in which the beam pipe width was varied from 75 to 300 mm while the height was held constant at 100 mm. The beam radius was 50 mm. Image coefficients were calculated from each simulation and the results plotted in Figure 9, along with Laslett's prediction for a centred beam between parallel plates. Laslett's image term is the solution that the simulation tends to as the ratio of horizontal to vertical beam pipe size becomes larger. As Laslett's solution is for infinite parallel plates this is to be expected. It is also clear that Laslett's solution is the "worst case scenario" and so represents a pessimistic estimate, useful for machine designs where one wants to err on the side of caution. It is also interesting that the incoherent image term approaches zero when the beam pipe ratio is 1.

Ng's solution was also compared with these results, also in Figure 9. As can be seen this value for the image coefficient had an excellent agreement with the simulation results.

ISBN 978-3-95450-173-1

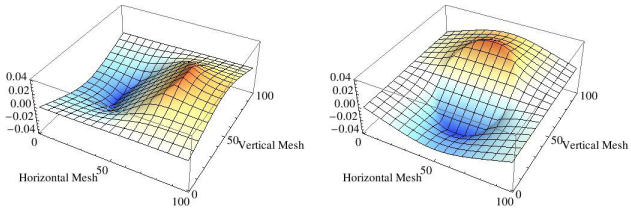

Figure 7: Fields produced by FFT solver: (left) horizontal and (right) vertical, units ϵ_0 V / mm.

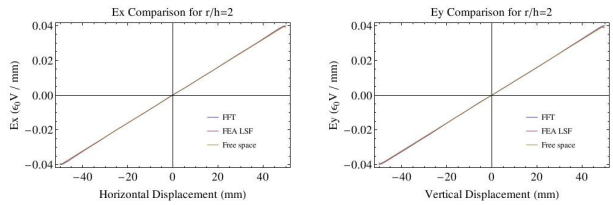

Figure 8: Fields produced by FFT and FEA solvers, compared with those for a KV beam in free space: (left) horizontal axis and (right) vertical axis.

Results for Off-Centred Beam

For these results, in addition to scanning the beam pipe aspect ratio between 0.75 and 3, the beam offset from centre was varied between 0 and 30 mm in steps of 5 mm. In each case the electric fields along the horizontal and vertical axes of the beam were recorded. For an off-centred beam the higher order image terms become significant. Baartman introduces the higher order image coefficients κ in [2] as follows

$$\frac{E_{yimage}}{4\lambda} = \epsilon_1 \frac{\hat{y}}{h^2} + \xi_1 \frac{\bar{y}}{h^2} + \kappa_{30} \frac{\bar{y}^3}{h^4} + \kappa_{21} \frac{\hat{y}\bar{y}^2}{h^4} + \kappa_{12} \frac{\hat{y}^2\bar{y}}{h^4} + \kappa_{03} \frac{\hat{y}^3}{h^4} + \ldots \quad (3)$$

A third order polynomial function with respect to $\hat{y}$ was fitted to the electric field obtained from the simulations. Further fitting was carried out to obtain functions with respect to $\bar{y}$ in order to obtain the values of the κ terms from Equation 3. Errors were calculated by generating 10 sets of additional values at beam pipe aspect ratios of 1 and 3, and the averages taken. These errors are representative of noise in the KV beam. The same method was used for the errors in the previous section.

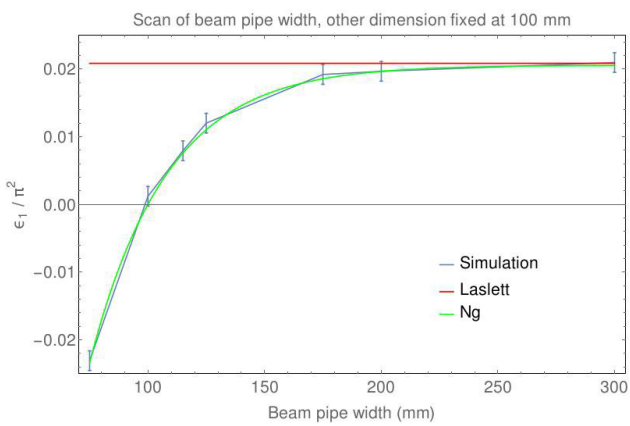

Figure 9: Results for a scan of beam pipe width from 75 - 300 mm, while height is held fixed at 100 mm. Laslett and Ng's image co-efficients for a centred beam compared with simulations.

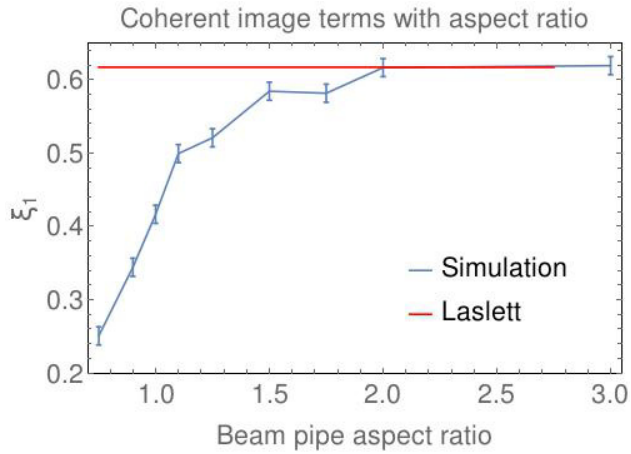

Figure 10: Laslett's image co-efficient for an off-centred beam, as a function of beam pipe aspect ratio from 0.75 - 3, compared with simulations.

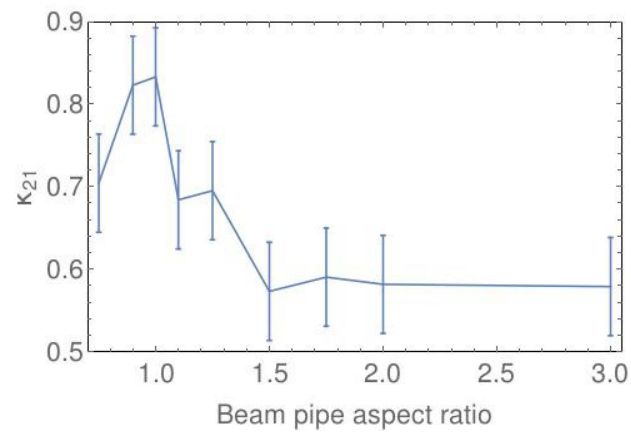

Figure 11: The higher order image term κ_{21} as a function of beam pipe aspect ratio from 0.75 - 3.

Figure 10 shows the value of the coherent image term ξ_1 as the beam pipe aspect ratio was scanned from 0.75 to 3. Laslett's value for the coherent term of $\frac{\pi^2}{16}$ is also included. As can be seen the simulation results approach Laslett's solution as the beam pipe aspect ratio becomes close to 2. However, where the ratio is around 1 the coherent term is nearer to half of this value.

Figure 11 shows the simulation results for the κ_{21} term from Equation 3. This is a quadrupole term whose strength is proportional to the square of the closed orbit offset. Rees, Prior and Baartman [1, 2] believed it could be responsible for some intensity dependent loss at ISIS. As can be seen from the plot, This term peaks where the beam pipe aspect

ISBN 978-3-95450-173-1

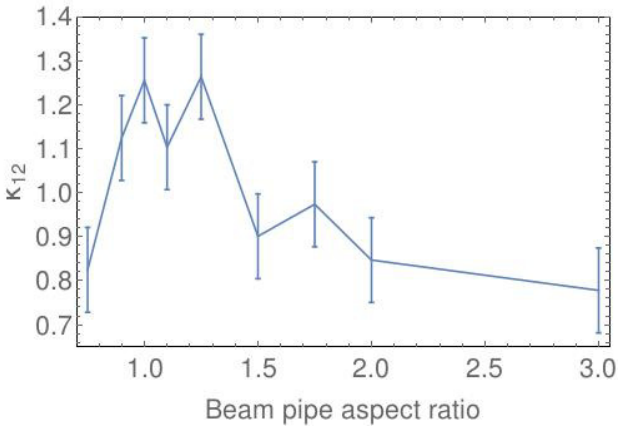

Figure 12: The higher order image term κ_{12} as a function of beam pipe aspect ratio from 0.75 - 3.

ratio is near to 1, and therefore where ϵ_1 and ξ_1 are smallest. While it is a small contribution to the overall image forces further work is required to explore its role in beam dynamics and loss.

There is also a sextupole term whose strength is proportional to the closed orbit offset, κ_{12}. The results for this term are shown in Figure 12. This term also peaks where the beam pipe aspect ratio is near to 1. Again as this is where ϵ_1 and ξ_1 are smallest there may be an observable effect on the beam dynamics.

In each of these cases the higher order image terms from the simulations did not tend to the parallel plates result which was obtained by Baartman. The reason for this is under investigation.

Image terms were also explored in the vertical plane (if the beam offset is in the horizontal plane). In the vertical plane ϵ_1 was equal to minus the value horizontally, as expected. ξ_1 and κ_{21} had values indistinguishable from zero, while κ_{30}, κ_{12} and κ_{03} all had finite values. This will be explored further in future work.

CONCLUSION

Theory for centred and off-centred beams in parallel plates, and for centred beams in rectangular geometry has been reviewed. Image term co-efficients, including the coherent and incoherent terms due to Laslett and Ng, as well as higher order terms due to Baartman have been identified.

A systematic simulation study including both FFT and FEA PIC solvers has been carried out to obtain these image terms numerically. There is a high level of agreement between the two functionally different solvers. The results of these simulations have been compared with theoretically obtained values.

For the case of a centred beam, a linear fit to the image terms is sufficient and this tends to Laslett's incoherent term as the beam pipe aspect ratio diverges. For a beam pipe aspect ratio greater than 2 Laslett's term is a close approximation to the image term. Ng's elliptical function solution for centred beams is an extremely good fit for the incoherent term generally, and describes it well when the beam pipe aspect ratio is near to 1.

When the beam is off-centre additional higher order image terms become evident. Laslett's coherent term is a good fit if the beam pipe aspect ratio is greater than 2. However when the beam pipe aspect ratio is near to 1, as it is on ISIS, this term is about half of Laslett's value.

Baartman describes the high order terms as κ terms. Of these, κ_{21} and κ_{12} have their greatest value when the aspect ratio is near to one, which is comparable to the situation on ISIS. While these terms are small it is possible that they have an effect on beam dynamics and this will be explored further.

Additionally there are equivalent image terms in the orthogonal (vertical) plane. Their contribution to beam dynamics likewise requires further study.

FURTHER WORK

High order image driving terms have been identified. The next step is to use these driving terms to predict the strength and stop-band width of associated resonances. The results of this analysis can then be compared with PIC simulations including the relevant dynamics. Ultimately it is hoped that any image related dynamic effects may be observed experimentally on ISIS.

Additionally further work is planned exploring Ng's elliptical function solution for off-centre beams, and seeing if this approach may provide another way to gain access to the high order image terms.

REFERENCES

[1] GH Rees and CR Prior, Image Effects on Crossing an Integer Resonance, Particle Accelerators Vol 48, p251, 1995.

[2] R Baartman, Betatron Resonances with Space Charge, Proceedings of Workshop in High Intensity Hadron Rings, Shelter Island, New York, 1998.

[3] LJ Laslett, On the Intensity Limitations Imposed by Transverse Space Charge Effects in Circular Accelerators, Proc. 1963 Summer Study on Storage Rings, Accelerators and Experimentation at Super-High Energies.

[4] KY Ng, Exact Solutions for the Longitudinal and Transverse Impedances of an Off-Centred Beam in a Rectangular Beampipe, Particle Accelerators Vol 16, p63, 1984.

[5] KY Ng, Physics of Intensity Dependent Beam Instabilities, p117, World Scientific, 2006.

[6] BG Pine et al, Set Code Developments and Space Charge Studies on ISIS, ICAP09, San Francisco, USA.

[7] BG Pine, Image Field Terms for 2D KV Beams in Rectangular Geometry at the ISIS Synchrotron, ISIS Technical Report, 2014.

ISBN 978-3-95450-173-1